

# Displacement Field and Elastic Energy of a Circular Twist Disclination for Large Deformations - an Example how to Treat Nonlinear Boundary Value Problems with Computer Algebra Systems

Alexander Unzicker

Pestalozzi-Gymnasium

Melssheimerstr. 11, D-81247 München, Germany

aunzicker@lrz.uni-muenchen.de

Karl Fabian

Department of Geosciences, University of Bremen

Box 330440, D-28334 Bremen, Germany

kfabian@uni-bremen.de

October 29, 2018

## Abstract

A circular twist disclination is a nontrivial example of a defect in an elastic continuum that causes large deformations. The minimal potential energy and the corresponding displacement field is calculated by solving the Euler-Lagrange-equations. The nonlinear incompressibility constraint is rigorously taken into account.

By using an appropriate curvilinear coordinate system a finer resolution in the regions of large deformations is obtained and the dimension of the arising nonlinear PDE's is reduced to two. The extensive algebraic calculations that arise are done by a computer algebra system (CAS). The PDE's are then solved by a difference scheme using the Newton-Raphson algorithm of successive approximations for multidimensional equations. Additional features for global convergence are implemented. To obtain basic states that are sufficiently close to the solution, a one dimensional linearized version of the equation is solved with a numerical computation that reproduces the analytical results of Huang and Mura (1970).

With this method, rigorous solutions of the nonlinear equations without any additional simplifications can be obtained. The numerical results show a contraction of the singularity line which corresponds to the well-known Poynting effect in nonlinear elasticity. This combination of analytical and numerical computations proves to be a versatile method to solve nonlinear boundary value problems in complicated geometries.

## 1 Introduction

Topological defects in elastic media usually generate large deformations which require finite elasticity for their description. The theory of nonlinear elasticity goes back to Cauchy (1827), and significant contributions came from Love (1927), Signorini (1930), and for the incompressible case, from Rivlin (1948a). For an introduction to nonlinear elasticity, the reader may consider Beatty (1987) or the standard textbooks Truesdell and Toupin (1960) and Truesdell and Noll (1965).

Topological defects, namely dislocations and disclinations, have been investigated by means of continuum theories (Kröner 1959; Kröner 1960) that were developed after the discovery of Kondo (1952) and Bilby,

Bullough, and Smith (1955) that dislocation density is related to the differential geometric concept of torsion. After the result of Frank (1949)<sup>1</sup> the elastic energy of topological defects in elastic continua has been considered in various publications on dislocations and disclinations (Eshelby 1949; Kroupa 1960; Huang and Mura 1970; Nabarro 1979). Puntigam (1996) discussed topological defects in a field theoretic context.

However, calculations of the elastic energy of topological defects have always been restricted to the linearized equations. In this case the problem can be treated using tensor analysis and stress function tensors of first and second degree (Kröner 1959). Two assumptions usually

<sup>1</sup>He showed that the energy increases relativistically with the dislocation velocity.

enter these approximations:

Firstly, one restricts to linear elasticity in the sense that shearing stresses are assumed to cause a state of simple shear in the material (as in Huang and Mura 1970).

Secondly, the energy is assumed to be a function of the distortion tensor that can be approximated by the gradient of the displacement field. Then, by applying Stoke's theorem, an integration over the boundaries only can be performed. Regarding the first point, however, it can be shown (e.g. Rivlin 1948c, p. 467), that in the general case shearing stresses alone cannot maintain a state of simple shear in the material. Also the second assumption is justified for *small* deformations only (Rivlin 1948c, p. 476). In the region close to the defect core, where the deformations are large the linear approximation fails to predict finite energies. Thus, these results are reasonable only outside the core region in where the energy density diverges.

Large deformations in crystals have been investigated rarely (Frank 1951), and if, not by means of analytical but by general topological methods (Rogula 1976) without considering the elastic energy.

There are several proposals how to treat nonlinear effects in elastic media with defects. Teodosiu (1982) obtained second-order effects for a straight screw dislocation by applying Willis' (1967; 1970) scheme which goes back to Signorini (1930). This requires, however, certain physical assumptions for every additional order of approximation. Guo (2001) modelled numerically the large deformations of a hyperelastic membrane. The cylindrical symmetry allowed a the reduction to a onedimensional PDE.

Lazar (2002a; 2002b) obtained solutions for edge and screw dislocations in an elastoplastic theory.

Povstenko (1995; 2000) has treated the twist disclination with a nonlocal modulus. Even if his method involves numerical integration, it is based on an analytical derivation of the stresses, and does not allow a contraction of the singularity line.

Here a more general approach is proposed: The total elastic energy, i.e. the integral over the energy density must be a minimum under variation of the displacement field  $\mathbf{u}$ . Additional constraints - like in the present case incompressibility - are included by means of a Lagrange multiplier. If the energy depends on first derivatives of  $\mathbf{u}$  only, this leads to Euler-Lagrange equations of second order, even if the method given here allows the treatment of higher order equations.

The general method outlined above is applied to a circular twist disclination (Huang and Mura 1970) in an incompressible hyperelastic continuum. It is a numerically automatized process for obtaining rigorous solutions of the nonlinear equations without special physical assumptions.

Section 2 gives a brief introduction to nonlinear continuum mechanics, followed by a description of the circu-

lar twist disclination. The appropriate coordinate system and the respective transformation of the the displacement vector is also explained there. All the numerical issues are addressed in section 3, and the results are discussed in section 4.

## 2 Analytical description

### 2.1 Basic concepts of nonlinear continuum mechanics

Nonlinear elasticity was founded in 1827 by Cauchy.

One assumes an undeformed, euclidian continuum with Cartesian coordinates  $\mathbf{X} = (X, Y, Z)$  (the so-called 'reference configuration') and attaches in every point a displacement vector  $\mathbf{u}$  that points to the coordinates  $\mathbf{x} = (x, y, z)$  of the deformed state ('configuration'):  $\mathbf{u} = \mathbf{x} - \mathbf{X}$ .

From  $\mathbf{u}$  one deduces a quantity that transforms the coordinates  $\mathbf{X}$  of the undeformed state to those  $\mathbf{x}$  of the deformed state: the deformation gradient

$$\mathbf{F} := \frac{\partial \mathbf{x}}{\partial \mathbf{X}},$$

or, in components,

$$\mathbf{F} := \begin{pmatrix} 1 + u_X & u_Y & u_Z \\ v_X & 1 + v_Y & v_Z \\ w_X & v_Y & 1 + w_Z \end{pmatrix}, \quad (1)$$

where  $(u, v, w)$  denote the components of  $\mathbf{u}$  and the subscripts differentiation. The symmetrical tensor

$$\mathbf{B} := \mathbf{F}\mathbf{F}^T, \quad (2)$$

is called (right) Cauchy-Green tensor. It is convenient to introduce the so-called *principal invariants* ( $I_1, I_2, I_3$ ) of a tensor that are defined as follows:

$$I_1 = \lambda_1 + \lambda_2 + \lambda_3 \quad (\text{trace}) \quad (3)$$

$$I_2 = \lambda_1\lambda_2 + \lambda_2\lambda_3 + \lambda_3\lambda_1 \quad (4)$$

$$I_3 = \lambda_1\lambda_2\lambda_3 \quad (\text{det}) \quad (5)$$

(the  $\lambda_i$  are the eigenvalues of  $\mathbf{B}$ ). Then, in general, the energy density  $W$  is a function of the principal invariants

$$W = W(I_1, I_2, I_3) \quad (6)$$

of the Cauchy tensor  $\mathbf{B}$  (e.g. Beatty 1987), and the stress tensor  $\mathbf{T}$  (defined as traction per surface element) is given by the constitutive equation

$$\mathbf{T} = \beta_1\mathbf{B} + \beta_0\mathbf{E} + \beta_{-1}\mathbf{B}^{-1} \quad (7)$$

with the  $\beta_i(I_1, I_2, I_3)$  being *functions* of the principal invariants. For small deformations, i.e. for  $I_1$ 's close to 1, and  $I_2, I_3$  close to 3, the  $\beta$ 's have a fixed values - that can be related to the known elastic *constants* in linear elasticity.

## 2.2 Incompressibility

The nonlinear condition of incompressibility is given by

$$I_3 = \lambda_1 \lambda_2 \lambda_3 = \det \mathbf{B} = (\det \mathbf{F})^2 = 1. \quad (8)$$

and *not*, as many texts on linear elasticity state,  $\operatorname{div} \mathbf{u} = \mathbf{0}$ . As a consequence, the elastic energy  $W$  depends on the principal invariants  $I_1$  and  $I_2$  of  $\mathbf{B}$  only and eqn. 6 reduces to

$$W = W(I_1, I_2) \quad (9)$$

In the present paper, the special case

$$W(I_1) = C(I_1 - 3) \quad (10)$$

is considered, which is called a *Neo-Hookean* material<sup>2</sup> where  $C$  is a constant.

## 2.3 Strain-Energy function expressed by displacements

Considering again a Cartesian coordinate system and taking into account (1), (3) and (10), the energy per unit volume for an incompressible, neo-Hookean material reads

$$W = C(\epsilon_{xx} + \epsilon_{yy} + \epsilon_{zz}), \quad (11)$$

where  $C$  corresponds to the shear modulus  $\mu$ ,<sup>3</sup> and the respective components of strain are given by (Cauchy 1827; Love 1927, p. 60 and Rivlin 1948b, p. 461)

$$\epsilon_{xx} = u_x + \frac{1}{2}(u_x^2 + v_x^2 + w_x^2) \quad (12)$$

$$\epsilon_{yy} = v_y + \frac{1}{2}(u_y^2 + v_y^2 + w_y^2) \quad (13)$$

$$\epsilon_{zz} = w_z + \frac{1}{2}(u_z^2 + v_z^2 + w_z^2). \quad (14)$$

Hereby  $\mathbf{u} = (u, v, w)$  denotes the displacement vector in  $x$ -,  $y$ -, and  $z$ -directions and  $u_x, u_y \dots$  etc. the respective partial derivatives.

## 2.4 Euler-Lagrange equations

The energy of the topological defect can be found by minimizing  $W$  under the variation of the displacement field  $\mathbf{u}$  which fulfill the correct spacial boundary conditions. In addition, the nonlinear constraint (8) is taken into account by means of a Lagrange multiplier  $\lambda$ . This requires the minimization of the Lagrangian

$$L = W + \lambda(\det \mathbf{F} - 1). \quad (15)$$

<sup>2</sup>This corresponds to the condition  $\beta_i = \text{const}$ . Note that in finite elasticity the energy density depends upon the functions  $\beta_i$ . Therefore, no general ‘canonical’ energy density exists.

<sup>3</sup>In an incompressible material,  $3C$  equals Young’s modulus  $E$ .

The Euler-Lagrange equations are thus obtained from

$$\frac{\partial L}{\partial u} - \frac{d}{dx} \frac{\partial L}{\partial u_x} - \frac{d}{dy} \frac{\partial L}{\partial u_y} - \frac{d}{dz} \frac{\partial L}{\partial u_z} = 0 \quad (16)$$

$$\frac{\partial L}{\partial v} - \frac{d}{dx} \frac{\partial L}{\partial v_x} - \frac{d}{dy} \frac{\partial L}{\partial v_y} - \frac{d}{dz} \frac{\partial L}{\partial v_z} = 0 \quad (17)$$

$$\frac{\partial L}{\partial w} - \frac{d}{dx} \frac{\partial L}{\partial w_x} - \frac{d}{dy} \frac{\partial L}{\partial w_y} - \frac{d}{dz} \frac{\partial L}{\partial w_z} = 0 \quad (18)$$

and

$$\frac{\partial(x + u, y + v, z + w)}{\partial(x, y, z)} - 1 = 0, \quad (19)$$

which is equivalent to (8). Using the special form of  $W$  from (11) without a Lagrange multiplier still leads to a linear PDE. Adopting  $W$  from (11) is not an essential simplification of the problem, since the condition (19) is the main nonlinearity. The principles of the following calculations apply in the same way to a nonlinear  $W$ .

## 2.5 Circular twist disclination

A circular twist disclination is a nontrivial example of a topological defect which enforces large deformations of an elastic continuum. The twist disclination can be realized as follows (see fig. 1):

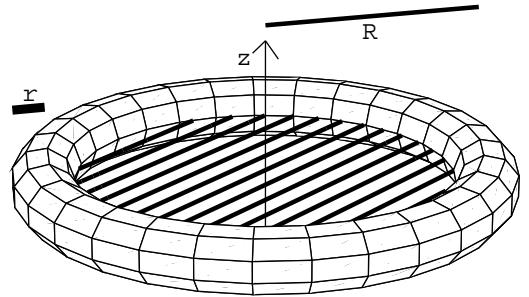


Figure 1: Schematic description how to produce a twist disclination in an elastic continuum. The solid torus (size  $R$ , thickness  $r$ ) is removed. Then the material is cut along the hatched surface. After twisting the cut faces by the amount of the Frank angle  $\Omega$ , the material is rejoined by gluing.

Imagine  $\mathbb{R}^3$  filled with elastic material and remove a solid torus centered around the origin and with  $z$  as symmetry axis (fig. 1). Cut the material along the surface bounded by the inner circle with radius  $R - r$  of the torus in the  $x - y$ -plane (hatched disk in fig. 1). The cut faces are twisted with respect to each other by the Frank angle  $\Omega$ , and glued together again.

If one shrinks the removed torus to a singularity line, in the limit  $r \rightarrow 0$  one obtains a circular twist disclination with radius  $R$ . In the subsequent computations, a sequence of finite values of  $r$  is used.

The above description of the twist disclination is equivalent to the one given by Huang and Mura (1970), who used however the term 'edge disclination'<sup>4</sup> to indicate that the Frank vector is perpendicular to the disclination line, in analogy to *edge dislocations* where the Burgers vector is perpendicular to the defect line. They investigated analytically the twist disclination in linear approximation.

## 2.6 Transformation to curvilinear coordinate systems

The boundary conditions for a specific problem can be formulated most conveniently in an appropriately chosen curvilinear coordinate system. Furthermore, different scale factors in this coordinate systems allow to pave the regions of interest - for example regions of large deformations - more densely with coordinate lines, which is of great numerical advantage. Frequently, one can use symmetries of a problem and reduce it to a lower dimension. The variety of orthogonal coordinate systems allows to design an appropriate system for nearly every problem, even for those with less symmetry. To give some examples, straight line defects may be modelled in a cylindrical system ( e.g. using a log-transformed radial component), closed line defects with various elliptic coordinate systems.

For the above described twist disclination, the toroidal system, as visualized in Fig. 2, is a suitable choice. To obtain the 3D-toroidal coordinate system from the 2-D bipolar system which is actually shown in Fig. 2, one must rotate the latter around the vertical axis.

The transformation is given by

$$x = \frac{\cos(\varphi) \sinh(\eta)}{-\cos(\vartheta) + \cosh(\eta)} \quad (20)$$

$$y = \frac{\sin(\varphi) \sinh(\eta)}{-\cos(\vartheta) + \cosh(\eta)} \quad (21)$$

$$z = \frac{\sin(\vartheta)}{-\cos(\vartheta) + \cosh(\eta)} \quad (22)$$

The parameter of the azimuthal rotation is  $\phi \in [0, 2\pi[$ , whereas the polar angle  $\vartheta$  ranges from 0 to  $\pi$ . The hyperbolic coordinate  $\eta$  ranges from  $-\infty$  (left focus) to  $\infty$  (right focus).

<sup>4</sup>To avoid confusion with screw and edge dislocations, the terms 'twist' and 'wedge' are commonly used for disclinations (deWit 1973a; 1973b; Zubov 1997). Rogula (1976) calls the circular twist disclination a 'third type of defect' and Unzicker (1996; 2000) a 'screw dislocation loop'. In any case, the twist disclination referred here causes locally a Volterra distortion of the 5th kind (see Puntigam 1996).

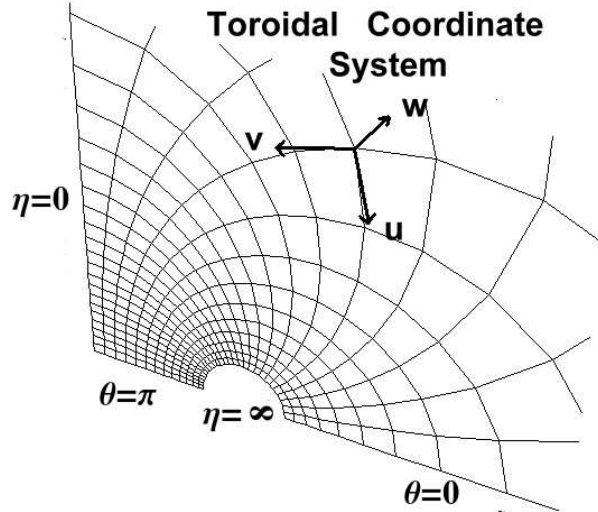


Figure 2: Toroidal coordinate system obtained by rotating a bipolar coordinate system around the  $z$ -axis ( $\eta = 0$ ). For symmetry reasons, only the region  $\eta > 0$  and  $0 < \vartheta < \pi$  (at  $\phi = 0$ ) is shown. The value  $\eta = \infty$  corresponds to a focus of the bipolar system or, after rotating around the  $z$ -axis, to a circular singularity line in the toroidal system.  $\eta = \vartheta = 0$  is the infinitely far point.

In the region in the vicinity of the circular singularity the Jacobian determinant is very small.  $\eta = \vartheta = 0$  corresponds to the infinitely far point. The components of the displacement vector in  $\eta$ -,  $\vartheta$ -, and  $\phi$ -direction are denoted as  $u$ ,  $v$  and  $w$ .

The transformation of differential operators like div and curl in curvilinear systems is long known (Love 1927, p. 54) and is easily done by CAS<sup>5</sup>.

To transform the expressions for the energy  $W$  and for the condition (19) in curvilinear coordinates, however, this is not sufficient, since the displacement vector components ( $u, v, w$ ) are involved. One has to take into account that the basis vectors in a curvilinear system are subject to change and differentiate them. This technique is well-known in differential geometry since it is needed for a curved spacetime in the general theory of relativity.

The spatial derivatives of the displacement vector  $\mathbf{u} = u^i = (u, v, w)$  are  $\frac{\partial \mathbf{u}}{\partial x^k}$ <sup>6</sup>. Taking into account the transformation of the basis vectors, the usual derivative has to be replaced by the 'covariant' derivative:

$$\frac{D}{Dx^k} u^i = \frac{d}{dx^k} u^i - \Gamma_{jk}^i u^j \quad (23)$$

The connection  $\Gamma_{jk}^i$  is calculated from the Jacobian matrix  $A_j^i$  ( $A_1^1 = \frac{\partial \eta}{\partial x}$  etc.) by

$$\Gamma_{jk}^i = B_k^i \frac{\partial}{\partial x^m} A_j^m, \quad (24)$$

<sup>5</sup>Here the *Mathematica*© package 'VectorAnalysis' has been used.

<sup>6</sup>In contrast to eqns. (16-18), ( $u, v, w$ ) and  $\frac{\partial}{\partial x^k}$  refers to  $\eta$ -,  $\vartheta$ -, and  $\phi$ -directions in the toroidal system.

$B_i^j$  is the inverse of  $A_j^i$  (Schouten 1954, p. 121ff.). Eqn. (24) has to be applied to *all* derivatives occurring in (16-19). This again is done by a CAS.

The transformation considerably complicates the equations. For example (11) becomes in toroidal coordinates

$$\begin{aligned}
W = & u_\eta(\cosh \eta - \cos \vartheta) + v_\vartheta(\cosh \eta - \cos \vartheta) + \quad (25) \\
& u(\operatorname{csch} \eta - \cos \vartheta \coth \eta) - 2v \sin \vartheta - u \sinh \eta + \\
& (w_\eta^2(\cosh \eta - \cos \vartheta)^2 + w_\vartheta^2(-\cos \vartheta + \cosh \eta)^2 + \\
& w^2(\cos \vartheta \cosh \eta - 1)^2 \operatorname{csch}^2 \eta + w^2 \sin^2 \vartheta + \\
& (v_\eta(\cosh \eta - \cos \vartheta) + u \sin \vartheta)^2 + \\
& (u_\eta(\cosh \eta - \cos \vartheta) - v \sin \vartheta)^2 + \\
& (u(\operatorname{csch} \eta - (\cos \vartheta \coth \eta)) - v \sin \vartheta)^2 + \\
& (v_\vartheta(\cosh \eta - \cos \vartheta) - u \sinh \eta)^2 + \\
& (u_\vartheta(\cosh \eta - \cos \vartheta) + v \sinh \eta)^2)/2
\end{aligned}$$

The transformation of eqns. (16-19), i.e. the full nonlinear PDE to solve, is not written out here,<sup>7</sup> they amount to a text file of about 30 *kB*. The extensive algebraic calculations necessary to transform the equations are done by a CAS.

## 2.7 Boundary conditions

The circular singularity of the twist disclination corresponds to  $\eta = \infty$ . A toroidal core  $\eta > \eta_{max}$  surrounding the singularity  $\eta = \infty$  is removed from the material. The chosen values of  $\eta_{max} = 2 \dots 3.625$  correspond to core radii  $r = 0.23 \dots 0.049$ . Since  $\eta = \vartheta = 0$  is the infinitely far point, only a region  $\eta > \eta_{min}$  and  $\vartheta > \vartheta_{min}$  is considered.

The distance  $R$  of the singularity line to the symmetry axis  $\eta = 0$  (the size of the defect) is set to 1.

The cylindrical symmetry of the problem in the coordinate  $\varphi$  reduces the 3D-problem to two dimensional one. Therefore,  $u$ ,  $v$  and  $w$  depend on  $\eta$  and  $\vartheta$  only. Furthermore, due to mirror symmetry  $\vartheta$  is restricted to the region  $0 < \vartheta < \pi$ .

The boundary values of  $u$ ,  $v$  and  $w$  are left free where ever possible in order to allow relaxing to the configuration of minimal energy. This is done at the surface of the torus surrounding the singularity at  $\eta = \eta_{max}$  (torus shown in fig. 1), and at  $\eta = 0$ . The boundary conditions at  $\vartheta = 0$  are enforced by the symmetry of the problem and at  $\vartheta = \pi$  by the 'cut-and-glue' condition with the Frank angle  $\Omega$ .

Thus at the disk defined by  $\vartheta = \pi$ ,  $v$  vanishes and  $u$  and  $w$  are fixed to a purely circular displacement corresponding to the Frank angle  $\Omega$  (see fig. 2). During energy minimization, the shape of the removed torus is kept fixed, otherwise the material could overlap, which is physically impossible. The boundary values  $w(\vartheta =$

<sup>7</sup>Note that minimization of  $W$  in the neo-Hookean case eqn. 11 still leads to a linear PDE. Only the constraint of incompressibility (8) enforces the substantial nonlinearity of the final PDE.

$\pi, \eta = \eta_{max}) = u(\vartheta = \vartheta_{min}, \eta = \eta_{max})$  implicitly implement this condition. Only for infinitesimal small values of  $\Omega$  the  $u$  component would vanish. In the linear approximation,  $u$ ,  $v$  and  $w$  vanish at  $\vartheta = 0$ . At the symmetry axis  $\eta = 0$  the condition of incompressibility causes the vanishing of  $u$  and  $w$  without an explicit setting to zero.

## 3 Numerical methods

### 3.1 Discretization with a difference scheme

The nonlinear Euler-Lagrange equations generated by the CAS are discretized on a twodimensional lattice by evaluating the coefficients  $\eta, \sin \vartheta$  etc. at every lattice point. The displacements and their derivatives are still maintained in analytic form. One obtains 4 variables (displacement vector  $\mathbf{u}$  and Lagrange multiplier  $\lambda$ ) at each of the  $n$  grid points. Therefore  $4n$  nonlinear equations have to be solved simultaneously.

### 3.2 Newton's method in multidimensions

The solutions of the arising nonlinear system are obtained by the Newton-Raphson method of successive approximations (Press 1993, chap. 9.7), which is a multidimensional extension of Newton's root finding algorithm. As in one dimension the algorithm starts from a basic state and uses first derivatives to iteratively calculate approximations of the solution.

The numerical computation of the  $4n$  derivatives of the Euler-Lagrange equations is however numerically inhibitive. This problem is solved by *analytically* differentiating the Euler-Lagrange equations at every lattice point with respect to the displacements  $u, v$  and  $w$  and their derivatives using a CAS. Thus the 18 quantities  $\lambda_\eta, \lambda_\vartheta, u_\eta, u_\vartheta, v_\eta, v_\vartheta, w_\eta, w_\vartheta, u_{\eta\vartheta}, v_{\eta\vartheta}, w_{\eta\vartheta}, u_{\vartheta\vartheta}, v_{\eta\eta}, w_{\eta\eta}, w_{\vartheta\vartheta}$  entering the Euler-Lagrange equations are discretized by difference molecules (Bronstein 1985, p. 767f.).

Only the simplest difference molecules are implemented to avoid instability of the Newton-Raphson method due to unrealistic smoothness assumptions. The possible grid dimensions do not allow to assume smoothness of the solution because the distortions in the vicinity of the toroidal core region usually become very large and higher order difference operators contain no next-neighbor coupling.

In addition, the difference scheme allows for a convenient formulation of the boundary conditions.

### 3.3 Global convergence

Although the above implementation is numerically very efficient, the global convergence of the direct multidimensional Newton-Raphson method is still not guaranteed. To obtain the global convergence of the algorithm one

usually defines a functional  $\mathbf{V}$  on the solution space as the square of the l.h. sides of eqns. 16-19. If the Newton step increases  $\mathbf{V}$  with respect to the previous state, the algorithm used here ‘walks back’ along the Newton direction looking for a one-dimensional local minimum of  $\mathbf{V}$ . (cfr. Press 1993, 9.7). The existence of such a local minimum is guaranteed, since at the basic state,  $\mathbf{V}$  by definition of the gradient decreases along the Newton direction. It turns out that convergence improves if the ‘walk back’ already is undertaken if  $\mathbf{V}$  decreased slightly, and the Newton step was ‘accepted’ only if  $\mathbf{V}$  decreases by less than a factor of 10. A factor 10 is easily reached in the vicinity of the solution, where the Newton-Raphson algorithm converges quadratically with distance. If the Newton step is accepted, its result is used as the basic state of the next iteration step around which the PDE is again linearized. In contrast to the advice given in Press (1993), it is found here that it is useful to minimize  $\mathbf{V}$  along the Newton direction precisely. Although this requires more function evaluations, it performs superior to taking some premature value for a new linearization.

For the one-dimensional minimization along the Newton direction, the golden sectio algorithm (Press 1993, chap. 10.1) is used. Where the function is sufficiently flat<sup>8</sup> (functionals  $\mathbf{V}$  at three points vary by less than a factor 1.2), the golden sectio is accompanied by parabolic interpolation (Press 1993, chap. 10.2) of the minimum. This combination, is found to perform quite well in finding solutions. Moreover, it is not sensitive to small variations of the above parameters.

### 3.4 Basic states

The success of the Newton-Raphson method critically depends on the basic state used for the first linearization. In the multidimensional case there is little hope that the algorithm directly converges to the solution without the above mentioned global-convergence methods. But even then the algorithm ends up in a local minimum if the first basic state is too far from the solution. There is for example, no chance to find a solution when starting with a nonspecialized basic state, e.g. with all variables set to zero. Sometimes linear approximations, e.g. states obtained by assuming small deformations, are chosen as basic states. In the present case, the linearized constraint of incompressibility  $\text{div } \mathbf{u} = 0$ , still is too far from reality to be used for constructing a first basic state. Thus, the incompressibility condition is directly implemented by using the symmetries of the toroidal coordinate system. In first approximation, it can be assumed that the displacement takes place along concentric circles with respect to the symmetry axis. Only for small displacements this corresponds to the tangential displacement of the linearized equation. Thus, no dilatation at all is allowed in the circular approximation. For practical rea-

<sup>8</sup>And if the point in the middle was not too excentric.

sons, only the component  $w$  of the displacement is varied. The components  $u$  and  $v$  are adjusted to meet the above requirement. This procedure requires to solve only a onedimensional linear PDE for calculating the basic states.

### 3.5 Interpolation and extrapolation

For finer grids and smaller core radii, it becomes increasingly difficult to find solutions by means of the above method.

It turns out that grid refinement by interpolating a previously found solution on a coarser grid is by far more efficient than starting with an independent new solution of the linearized system. The interpolation is performed by a 2D-spline algorithm (Press 1993, chap. 3.6) and the interpolated function – evaluated at the refined grid – is taken as new basic state. Starting from this state, a new solution usually is obtained by Newton-Raphson. However, this refined solution still has the same core radius as the previous coarse solution. For extending the grid towards smaller core radii, that is to larger  $\eta_{max}$ , a very efficient method is to attach one lattice line to the old solution by linear *extrapolation*, and to use this extended solution again as a new basic state. All solutions for very small core radii have been obtained in this way.

### 3.6 Matrix inversion and function evaluation

Matrix size increases very rapidly with the number of grid points. For example, the four functions  $(\lambda, u, v, w)$  on a  $30 \times 30$  lattice lead to a  $3600 \times 3600$  matrix with almost  $13 \times 10^6$  coefficients, which has to be inverted at every Newton step. Since the matrix is sparse, the inversion is more efficiently done by specialized sparse matrix algorithms. Here the corresponding packages of *MatLab*© are applied over a data exchange interface with *Mathematica*©.

Since CAS are slow in evaluating trigonometric functions, the evaluation is done by an external *C* routine. This speeds up the computation of the matrix coefficients by a factor 10 as compared to the CAS.

With this features, satisfactory results are obtained by running the program on a usual PC.

## 4 Results

### 4.1 Linear approximation

In linear approximation the twist disclination can be treated analytically. Huang and Mura (1970) have found that the total elastic energy is

$$W = \left(\frac{1}{3}\mu \Omega^2 R^3\right) \left\{ \left[ 2 + \left(1 - \frac{r}{R}\right)^2 \right] K \left(1 - \frac{r}{R}\right) - \right. \quad (26) \\ \left. 2 \left[ 1 + \left(1 - \frac{r}{R}\right)^2 \right] E \left(1 - \frac{r}{R}\right) \right\},$$

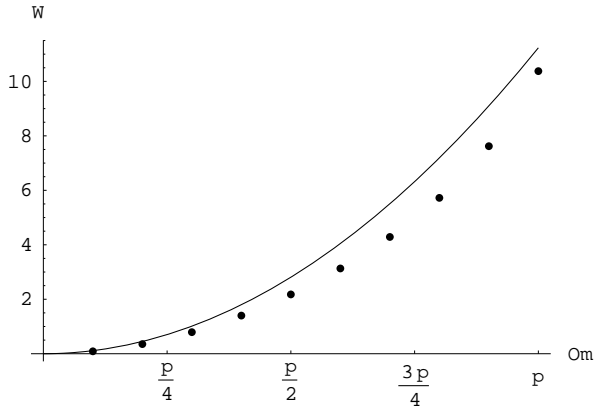


Figure 3: Comparison of the numerical results for the linear approximation (filled circles) with the analytical results (solid line) of Huang and Mura (1970) in case of a core radius of 0.09 ( $\eta_{max} = 3$ ,  $\eta_{min} = \vartheta_{min} = 0.05$ ,  $R = 1$ ,  $\mu = 3$ ). The defect energy increases with the amount of the Frank angle  $\Omega$  (ranging from 0 to  $\pi$ ). For small  $\Omega$ , the results agree.

where  $K$  and  $E$  denote the complete elliptic integral of the first and second kind. Eqn. 26 can be approximated by

$$W = \frac{1}{3}\mu \Omega^2 R^3 \left( \frac{1}{2} \log(8R/r) - \frac{4}{3} \right). \quad (27)$$

This result is used to test the algorithm for calculating the basic states (section 3.4). Fig. 3 shows that numerical and analytical results agree for small  $\Omega$ . The predicted  $\Omega^2$ -dependence in eqn. 26 is reproduced by the linear algorithm.

For larger values of  $\Omega$ , however, the energies calculated numerically lie below the parabola of Huang and Mura (1970). This illustrates the two aspects of a linear approximation: both in the analytical and in the numerical treatment shear stresses are assumed to cause pure shear, but the latter approach lifts the small-deformation assumption by taking the energy function (11).

## 4.2 Solutions of the complete nonlinear PDE

The linear assumption of shear stresses causing shear deformations only is lifted now. The solutions of the fully nonlinear equation presented here are constraint to the the case  $\Omega = \pi$  where very large deformations occur. Fig. 4 visualizes these deformations for a core radius  $r = 0.23$ . The other parameters are  $\mu = 3$ ,  $R = 1$ ,  $\eta_{min} = \vartheta_{min} = 0.05$ . The dotted line indicates the singularity. Fig. 2 shows the corresponding undeformed state.

The components of the displacement vector  $u$ ,  $v$  and  $w$ , for the same parameters as in fig. 4, are shown in fig. 5. Note that the grid shown in fig. 5 is equidistant in the toroidal coordinates  $\eta$  and  $\vartheta$ , but not in a cartesian frame, as it is evident from figs. 2 and 4. There,

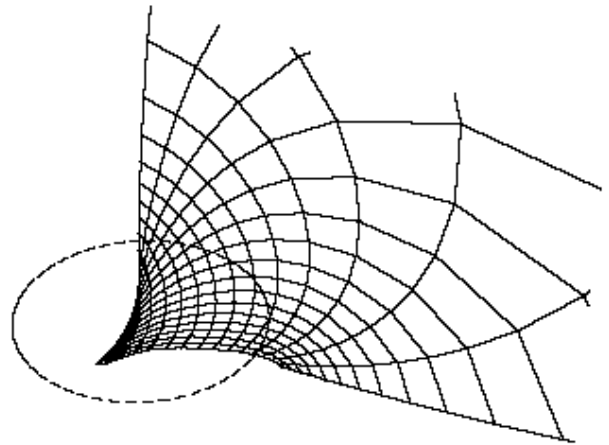


Figure 4: Solution of the nonlinear PDE. The respective undistorted state is shown in fig. 2, with singularity as dotted line. A very large deformation with a Frank angle  $\Omega = \pi$  is implemented by twisting the lower boundary  $\vartheta = \pi$  by the amount of  $\pi/2$ . The lower part  $-\pi/2 < \vartheta < 0$  (not shown here) is twisted in the opposite direction. The core radius is  $r$  about 0.23,  $\eta_{max} = 2$ ,  $\eta_{min} = \vartheta_{min} = 0.05$ .

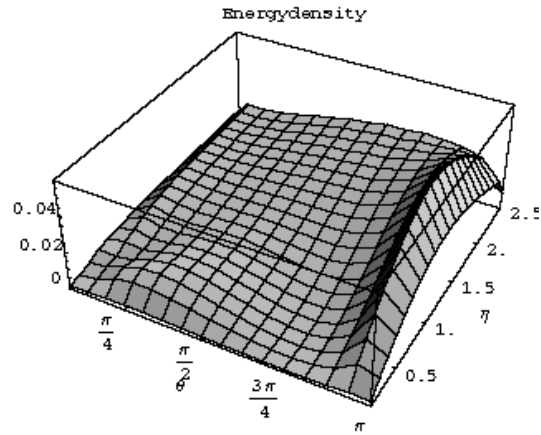
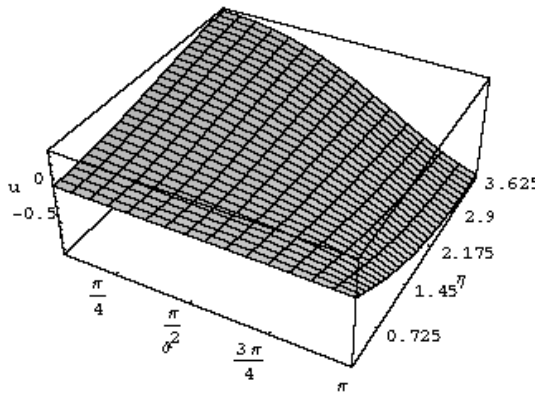
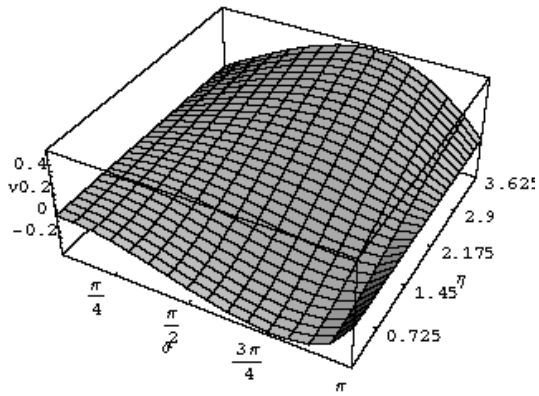


Figure 6: Distribution of the elastic energy for an circular twist disclination with  $\eta_{max} = 2.5$  (equivalent to  $r = 0.145$ ), and  $\eta_{min} = \vartheta_{min} = 0.05$ .



the lattice spacing is much finer in the region of large deformations.

Even if it demands quite a lot of imagination, the reader should verify that the displacement components in fig. 5, attached to fig. 2, yield indeed the deformation fig. 4.

In fig. 6 ( $r = 0.145$ ) the distribution of the elastic energy plotted. At each grid point the energy density, weighted by the corresponding toroidal volume element, is shown. Most of the energy is stored in the region nearby the cut surface, where its density is greater than in the vicinity of the core region  $\eta = \eta_{max}$ . This effect is even more pronounced for smaller core radii  $r$ .

### 4.3 Elastic energy

Fig. 7 shows the total elastic energy of a circular twist disclination in function of  $\eta_{max}$  which parametrizes the core radius.

Using the global minimization techniques discussed above, solutions over a wide range from  $\eta_{max} = 2.0$  (which corresponds to  $r = 0.23$ ) to  $\eta_{max} = 3.625$  ( or  $r = 0.049$ ) are found. Fig. 7 shows the dependence of the energy (filled circles) from  $\eta$ .<sup>9</sup> It is considerably reduced in comparison to the linear approximation of Huang and Mura (1970) (solid line). Although from numerical results like those of fig. 7 it cannot be deduced that the energy approaches a finite value in the limit  $r \rightarrow 0$ , fig.6 suggests the energy density decreases sufficiently for convergence.

The total elastic energies shown in fig. 7 are calculated from a lattice of 16 points in  $\vartheta$ -direction, whereas the number of points in  $\eta$ -direction ranged from 17 to

<sup>9</sup> $\eta$  stands for  $\eta_{max} + \eta_{min}$  here.

Figure 5: vector components  $u(\eta, \vartheta)$ ,  $v(\eta, \vartheta)$  and  $w(\eta, \vartheta)$  for the solution fig. 4 (core radius  $r = 0.23$ ).



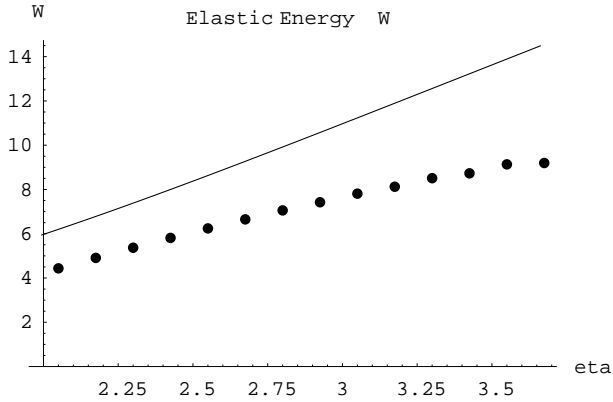


Figure 7: Dependence of the total elastic energy of circular edge disclinations for  $\eta_{max} = 2.0$  ( $r = 0.23$ ) to  $\eta_{max} = 3.625$  ( $r = 0.049$ ). The filled circles are obtained from the nonlinear modelling, the solid line shows the analytic result of Huang and Mura (1970). The cutoff of the infinitely far point was  $\eta_{min} = \vartheta_{min} = 0.05$ , which corresponds to a distance of about 20 from the origin. There were 16 lattice points in  $\vartheta$ -direction and a range from 17 to 30 for  $\eta$ .

30. The outer limit of the modelled region is defined by  $\eta_{min} = \vartheta_{min} = 0.05$ . Other solutions with a different number of grid points, and smaller values for  $\eta_{min}$  and  $\vartheta_{min}$  (0.01, 0.02) showed only a very slight dependence on these parameters.

#### 4.4 Poynting effect

The solutions of the nonlinear case show a characteristic phenomenon which only occurs in the elasticity theory of finite deformations, the so-called Poynting effect.

The Poynting effect in its classic form is (Truesdell and Noll 1965, p. 193): ‘When an incompressible cylinder, free on its outer surface, is twisted, it experiences an *elongation* ultimately proportional to the square of the twist.’

To illustrate the difference between the linear approximation and the nonlinear solution, fig. 8 and 9 show the vector component  $v$  in  $\vartheta$ -direction for  $r = 0.09$ . In the region close to  $\eta = 0$ , i.e. in the vicinity of the symmetry axis,  $v$  has negative values and the displacement vector is pointing upwards in the region where  $z > 0$ . (cfr. fig. 2). By mirror symmetry it points downwards in the region of  $z < 0$  ( $-\pi < \vartheta < 0$ ). As a consequence the material is stretched and incompressibility forces the central region close to the cut surface to contract.

The elongation indicated for  $z > 0$  is observed in the nonlinear case only. It is a displacement normal to the plane on which the stress is induced (the cut surface). In the linear case from the assumption of pure shear caused  $v = 0$  at the symmetry axis (fig.8).

The Poynting contraction apparently approaches a

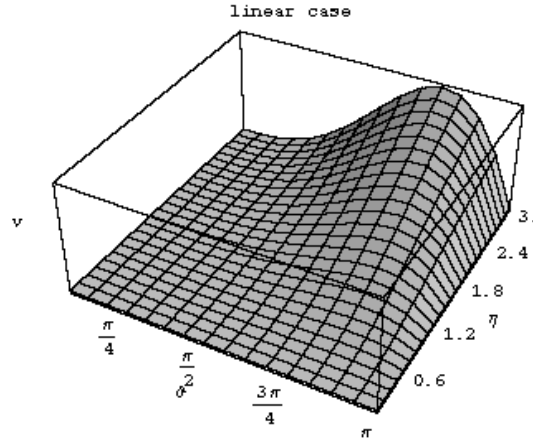


Figure 8: Example of a small core radius  $r = 0.09$ . Vector component  $v$  in  $\vartheta$ -direction for a solution of the linearized equations.

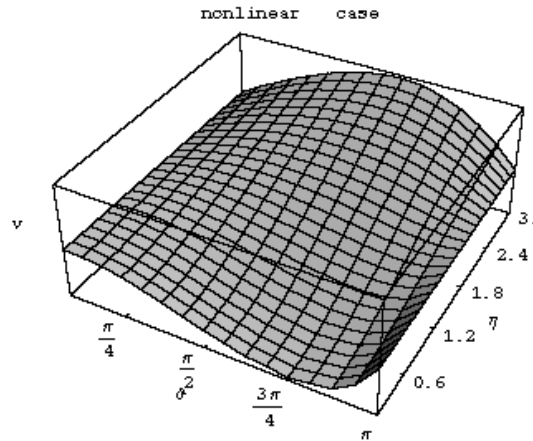


Figure 9: As fig.8, but for the nonlinear case. In the region nearby  $\eta = 0$ , i.e. in the vicinity of the symmetry axis,  $v$  has negative values. that means it is pointing upwards. The material is stretched and the cut surface contracts.

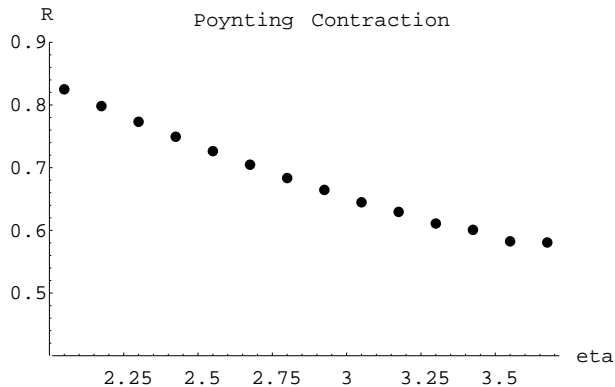


Figure 10: Poynting contraction as fraction of the original size of the defect. The contraction seems to reach a lower bound at .58, at a core radius of 0.049, which corresponds to  $\eta_{max} = 3.625$ .

positive lower limit for very small core radii  $r$ . The results shown in fig. 10 suggest that the contraction does not fall below 58% of the original radius.

#### 4.5 Problems

For both  $\eta_{max} < 2.0$  and  $\eta_{max} > 3.75$  it becomes increasingly difficult to find solutions of the nonlinear equations. In the first case the difficulty appears to be related to the imposed boundary conditions which fix the torus diameter  $r$  (i.e. the core radius). In the second case the Poynting contraction leads to a net change in the torus volume, which apparently leads to numerical problems.

On the other hand, for small core radii, the program finds solutions which satisfy the numerical convergence criterium, but show a physically unreasonable zigzag-pattern in the displacements. Possibly they occur in huge deformations (a volume element of the size of the core radius becomes stretched to the length of the singularity line) become numerically untractable at least with the present method ('relatively' simple coordinate system). However, there still may be a deeper physical reason for this instability.

A simpler analogue to the circular edge disclination in case of large deformations is a twisted rubber band. Everyday experience shows that while the Poynting effect only slightly elongates the band, the band spontaneously loses its axial symmetry and coils up as soon as the twist surpasses a critical value.

In case of the edge disclination, the present model – which essentially depends on rotational and mirror symmetry is not able to correctly model such a transition. It is therefore not astonishing that meaningful solutions are found up to a maximal  $\eta_{max}$  only.

## 5 Conclusions

By combining analytical and numerical approaches, a general method for obtaining rigorous solutions of nonlinear boundary value problems with nontrivial geometries has been developed.

With this new method, for the first time the fully nonlinear problem of a circular twist disclination in an hyperelastic incompressible material could be treated.

While the extensive calculations necessary for formulating Euler-Lagrange-equations in a curvilinear coordinate system were done by the computer algebra system, the solution of the discretized equations was obtained by the Newton-Raphson method with additional global convergence features. The results give a nonlinear correction to the total elastic energy obtained in analytical treatments (Huang and Mura 1970). Moreover, the method allowed for the first time to model the contraction of the singularity line and to observe the Poynting effect, which is characteristic for large deformations in finite elasticity. An application of the outlined method to other nonlinear PDE's with boundary value problems in several dimensions seems possible.

**Acknowledgement.** We are grateful to Dr. Markus Lazar for hints to the literature.

## References

- Beatty, M. F. (1987). Topics in finite elasticity: Hyperelasticity of rubber, elastomers, and biological tissues - with examples. *Appl. Mech. Rev.* 40, 1699–1733.
- Bilby, B. A., R. Bullough, and E. Smith (1955). Continuous distributions of dislocations: a new application of the methods of non-riemannian geometry. *Proc. Roy. Soc. London, Ser. A* 231, 263–273.
- Bronstein, I. N. (1985). *Taschenbuch der Mathematik* (22 ed.). Leipzig: Teubner.
- Cauchy (1827). De la pression ou tension dans un corps solide; sur la condensation et la dilatation des corps solides; sur les equations qui expriment les conditions d'équilibre ou les lois de mouvement interieur d'un corps solide. *Exercices de mathématique*.
- deWit, R. (1973a). Theory of disclinations: II. continuous and discrete disclinations in anisotropic elasticity. *J. Res. Nat. Bur. Standards* 77A(1), 49–100.
- deWit, R. (1973b). Theory of disclinations: III. continuous and discrete disclinations in isotropic elasticity. *J. Res. Nat. Bur. Standards* 77A(3), 359–368.
- Eshelby, J. D. (1949). Uniformly moving dislocations. *Proceedings of the Physical Society London A* 62, 307–314.

- Frank, C. F. (1949). On the equations of motion of crystal dislocations. *Proceedings of the Physical Society London A* 62, 131–134.
- Frank, C. F. (1951). Crystal dislocations - Elementary concepts and definitions. *Philos. Mag. VII Ser.* 42, 809–819.
- Guo, X. P. (2001). Large deformation analysis for a cylindrical hyperelastic membrane of rubber-like material under internal pressure. *Rubber Chemistry and Technology* 74(1), 100–115.
- Huang, W. and T. Mura (1970). Elastic field and energies of a circular edge disclination and a straight screw disclination. *Journal of Applied Physics* 41(13), 5175–5179.
- Kondo, K. (1952). *RAAG Memoirs of the unifying study of the basic problems in physics and engineering science by means of geometry*, Volume 1. Tokio: Gakujutsu Bunken Fukyu-Kay.
- Kröner, E. (1959). *Kontinuumstheorie der Versetzungen und Eigenspannungen*. Springer.
- Kröner, E. (1960). Allgemeine Kontinuumstheorie der Versetzungen und Eigenspannungen. *Arch. Rat. Mech. Anal.* 4, 273–334.
- Kroupa, F. (1960). Circular edge dislocation loop. *Czechoslovakian Journal of Physics B* 10, 285–193.
- Lazar, M. (2002a). A nonsingular solution of the edge dislocation in the gauge theory of dislocations. *e-print archive cond-mat/0208360*.
- Lazar, M. (2002b). Screw dislocations in the field theory of elastoplasticity. *e-print archive cond-mat/0203058*.
- Love, A. E. H. (1927). *The Mathematical Theory of Elasticity* (2 ed.). Dover Reprint.
- Nabarro, F. (1979). *Dislocations*. North-Holland.
- Povstenko, Y. Z. (1995). Circular disclination loops in nonlocal elasticity. *Journal of Physics D- Applied Physics* 28(1), 105–111.
- Povstenko, Y. Z. (2000). Circular disclination loops in nonlocal elasticity. *Int. J. of Solids and Structures* 37(44), 6419–6432.
- Press, W. H. (1993). *Numerical Recipes in C - the art of scientific computing* (2nd ed.). Cambridge: Cambridge Univ. Pr.
- Puntigam, R. A. (1996). Volterra distortions, spinning strings, and cosmic defects. *Class. Quantum Grav.*
- Rivlin, R. S. (1948a). Large elastic deformations of isotropic materials. I.- VI. *Phil.Trans.Roy.Soc.London A* 240, 459–508; A 241, 379–397; A 242 (1949), 173–195; Proc.Roy.Soc.London A 195 (1949), 463–473.
- Rivlin, R. S. (1948b). Large elastic deformations of isotropic materials. I. Fundamental concepts. *Phil.Trans.Roy.Soc.London A* 240, 459–90.
- Rivlin, R. S. (1948c). Large elastic deformations of isotropic materials. II. Some uniqueness theorems for pure homogeneous deformations. *Phil.Trans.Roy.Soc.London A* 240, 491–508.
- Rogula, D. (1976). Large deformations of crystals, homotopy and defects. In G. Fichera (Ed.), *Trends in applications of pure mathematics to mechanics*, pp. 311–331. London: Pitman.
- Schouten, J. A. (1954). *Ricci-Calculus*. New York: Springer.
- Signorini, A. (1930). *Proc. 3rd Int. Congr. Appl. Mech. Stockholm* 2(14), 80.
- Teodosiu, C. (1982). *Elastic models of crystal defects*. Berlin: Springer.
- Truesdell, C. and W. Noll (1965). *The Non-Linear Field Theories of Mechanics*, 2nd ed. 1992 (2nd ed.). Berlin New York: Springer.
- Truesdell, C. and R. Toupin (1960). The classical field theories. In S. Flügge (Ed.), *Handbuch der Physik*, Volume III/1, pp. 266–793. Berlin: Springer.
- Unzicker, A. (1996). Teleparallel space-time with defects yields geometrization of electrodynamics with quantized sources. *e-print Archive gr-qc/9612061*.
- Unzicker, A. (2000). What can physics learn from continuum mechanics ? *e-print Archive gr-qc/0011064*.
- Willis, J. R. (1967). *Int. J. of Engineering Science* 5, 171.
- Willis, J. R. (1970). Stress fields produced by dislocations in anisotropic media. *Philosophical Magazine* 21, 931–949.
- Zubov, L. M. (1997). *Nonlinear theory of dislocations and disclinations in elastic bodies*. Berlin: Springer.